REPORT DOCUMENTATION PAGE

Form Approved
OMB No. 0704-0188

1. REPORT DATE *(DD-MM-YYYY)*

2. REPORT TYPE
Technical Papers

3. DATES COVERED *(From - To)*

4. TITLE AND SUBTITLE
Please see attached

5a. CONTRACT NUMBER

5b. GRANT NUMBER

5c. PROGRAM ELEMENT NUMBER

6. AUTHOR(S)

5d. PROJECT NUMBER
2302

5e. TASK NUMBER
M1G2

5f. WORK UNIT NUMBER
346120

7. PERFORMING ORGANIZATION NAME(S) AND ADDRESS(ES)

Air Force Research Laboratory (AFMC)
AFRL/PRS
5 Pollux Drive
Edwards AFB CA 93524-7048

8. PERFORMING ORGANIZATION REPORT

9. SPONSORING / MONITORING AGENCY NAME(S) AND ADDRESS(ES)

Air Force Research Laboratory (AFMC)
AFRL/PRS
5 Pollux Drive
Edwards AFB CA 93524-7048

10. SPONSOR/MONITOR'S ACRONYM(S)

11. SPONSOR/MONITOR'S NUMBER(S)
Please see attached

12. DISTRIBUTION / AVAILABILITY STATEMENT

Approved for public release; distribution unlimited.

13. SUPPLEMENTARY NOTES

14. ABSTRACT

20030205 138

15. SUBJECT TERMS

16. SECURITY CLASSIFICATION OF:

a. REPORT	b. ABSTRACT	c. THIS PAGE	17. LIMITATION OF ABSTRACT	18. NUMBER OF PAGES	19a. NAME OF RESPONSIBLE PERSON
Unclassified	Unclassified	Unclassified	A		Leilani Richardson

19b. TELEPHONE NUMBER *(include area code)*
(661) 275-5015

G2

MEMORANDUM FOR PRS (In-House Publication)

FROM: PROI (STINFO) 22 May 2002

SUBJECT: Authorization for Release of Technical Information, Control Number: **AFRL-PR-ED-TP-2002-129**
C.W. Smith; D.M. Constantinescu (V.PolyTech); C.T. Liu (PRSM), "Stress Intensity Factors and Crack Path for Cracks in Photoelastic Motor Grain Models"

ASME 2002 Winter Meeting **(Statement A)**
(New Orleans, LA, 17-22 ____ 2002) **(Deadline = 20 June 2002)**

1. This request has been reviewed by the Foreign Disclosure Office for: a.) appropriateness of distribution statement, b.) military/national critical technology, c.) export controls or distribution restrictions, d.) appropriateness for release to a foreign nation, and e.) technical sensitivity and/or economic sensitivity.
Comments: ____

Signature ____ Date ____

2. This request has been reviewed by the Public Affairs Office for: a.) appropriateness for public release and/or b) possible higher headquarters review.
Comments: ____

Signature ____ Date ____

3. This request has been reviewed by the STINFO for: a.) changes if approved as amended, b) appropriateness of references, if applicable; and c.) format and completion of meeting clearance form if required
Comments: ____

Signature ____ Date ____

4. This request has been reviewed by PR for: a.) technical accuracy, b.) appropriateness for audience, c.) appropriateness of distribution statement, d.) technical sensitivity and economic sensitivity, e.) military/ national critical technology, and f.) data rights and patentability
Comments: ____

APPROVED/APPROVED AS AMENDED/DISAPPROVED

PHILIP A. KESSEL Date
Technical Advisor
Space and Missile Propulsion Division

STRESS INTENSITY FACTORS AND CRACK PATHS FOR CRACKS IN PHOTOELASTIC MOTOR GRAIN MODELS

C. W. Smith[1], D. M. Constantinescu[1] and C. T. Liu[2]

[1] Department of Engineering Science and Mechanics
Virginia Polytechnic Institute and State University
Blacksburg, Virginia 24061

[2] Air Force Research Laboratory, PRSM
10 E. Saturn Blvd.
Edwards AFB, California 93524-7680

ABSTRACT

Computational analysis and two dimensional tensile tests on single motor grain fins suggest that cracks in fin tips are most likely to originate at the coalescence of the fin end tip radius with a small radius emanating from the side of the fin. Prior studies have indicated that under internal pressure, cracks on the fin axis are subject to similar stress peaks and may grow more readily than the former types due to an absence of shear modes. The present study focuses upon two types of cracks emanating from the former location called "off-axis" cracks and attempts to differentiate from the two types by their paths and SIF values, determined by the frozen stress photoelastic method.

INTRODUCTION

Tension tests on pie shaped sections of a generic motor grain model containing a single fin at AFRL revealed that cracks initiated at the confluence of the central fin tip radius and the edge radius. A preliminary photoelastic study of an uncracked fin has shown (Smith, Constantinescu and Liu, 2001) that the peak stress on the fin axis tip is nearly as great as at the off-axis position. In order to study the growth of cracks from the two above noted positions and measure the stress intensity factor (SIF's) at various locations along the crack borders, a series of frozen stress (Appendix A) photoelastic experiments were carried out on generic six finned motor grain models containing two cracks in each model (Fig. 1). The cracks were assumed to grow independently of each other.

THE EXPERIMENTS

The cracks located on the axis of symmetry of a fin were planar, grew in that plane and exhibited Mode I fields all around the flaw border. As such, they were Class I (Cotterell, 1965) cracks throughout their growth and grew readily under internal pressure revealing no unusual effects. On the other hand, the cracks which were initiated at the confluence of the R1.3 and R11 values (Fig. 1) were initially nonplanar and proceeded to turn under internal pressure, exhibiting Class II crack behavior until finding their Class I direction for further growth. Crack growth was retarded by this turning effect which involved the elimination of shear modes present during turning. This study focuses on two types of such cracks called off-axis cracks.

Two kinds of off-axis cracks were used, those entering the model *normal* to the fin surface and those entering the model *parallel* to the fin axis. The first type was made by drilling a small hole opposite the fin to be cracked, (Fig. 2) and inserting a shaft with two blades such that the blade producing the crack was *normal* to the fin surface. Typical cracks formed in this way with the blade held normal to the surface are shown in Fig. 3.

In Model 4, all of the crack growth was under mixed mode (Modes I & II) loading and both modes existed everywhere when growth was stopped except near the fin surface where only Mode I existed. The crack is thus still a Class II crack. In Model 8-i, the crack has grown out of both Modes II and III, becoming parallel to the fin axis, and exhibited only a Mode I SIF along the crack border. The river marks indicated that Mode III was present earlier. They are exacerbated by slight tilting of the blade with respect to the fin surface. Retardation of growth along the crack front by Mode III is shown in Model 8 in the region of the river marks.

Fig. 4 shows a typical starter crack and its growth when the blade is held *parallel* to the fin axis. A small damaged region is shown at entry into the model but the crack quickly orients itself parallel to the fin axis under internal pressure and exhibited pure Mode I all around the crack front as a Class I crack. A few river marks indicate the presence of some Mode III which was eliminated during growth.

It appeared that large displacements normal to the crack surface were responsible for the river marks so no calculations were made where they were near the surface in any of the cracks.

Since turning occurs above the critical temperature (T_c) of the material, the turning effect is gradual (Smith, Constantinescu and Liu, 2001), and not a kink.

In examining the results, it appears that the presence of the river markings exerted a substantial effect upon the SIF calculations when the data were taken before significant crack growth has occurred after turning. This was due to several factors:

i. The projected crack shape deviated significantly from a semi-ellipse during and just after turning (Fig. 3, Model 8-i)

ii. The fracture surface was not smoothly continuous.

iii. Where the river markings extended to the crack front, one expects large non-linear Mode III effects (Fig. 3 Model 8-i).

vi. Crack growth beyond turning was not sufficient to eliminate the significance of items i through iii for shorter cracks and so substantial scatter resulted in the SIF values in these cases, and are not reported herein.

RESULTS

A two parameter method developed earlier (Smith and Kobayashi, 1993) was used to convert near tip stress fringe patterns into SIF values. The algorithms for Modes I and II are given in Appendix B. No Mode III calculations were made due to the large out of surface deformations. Normalized values of the SIF's (ie. F_i) were computed as indicated in Table I assuming that the cracks were semi-elliptic and planar. This was nearly true for the cracks entering the body *parallel* to the fin axis. However, for cracks entering the body *normal* to the fin surface, cracks were neither planar nor semi-elliptic as noted above.

For the cases where the cracks were inserted parallel to the fin axis, all of the cracks were Class I and pure Mode I and results are plotted in Fig. 5. These cracks exhibited negligible turning and their final depths included much more growth (25 to 75% of the final crack depth) than those initiated normal to the fin surface at the same off-axis locations. The data scatter are all within the experimental accuracy of 6%.

SUMMARY

A series of frozen stress photoelastic experiments were conducted on internally pressurized generic six finned motor grain models. Starter cracks were initiated by sharp blades which produced real cracks by wedging the material open. Crack growth and SIF values were measured along the flaw borders. Results showed that off-axis cracks produced shear modes which retarded the crack growth relative to symmetric cracks which initiated as Class I cracks under pure Mode I. After turning, the off-axis cracks, initially Class II cracks, became Class I cracks and grew parallel to the fin axis. Results showed that from a/t of 0.20 to 0.68, the normalized SIF decreased with increasing depth.

ACKNOWLEDGEMENTS

The authors gratefully acknowledge the support of this work by ERC Inc. through AFRL under P.O. RPO10230.

REFERENCES

Cotterell, B., "On Brittle Fracture Paths," *International Journal of Fracture Mechanics,* Vol. 1, pp. 96-103, 1965.

Smith, C. W. and Kobayashi, A. S., " Experimental Fracture Mechanics," *Handbook on Experimental Mechanics,* (2nd Revised Ed.) Chapter 20, pp. 905-968, 1993.

Smith, C. W., Constantinescu, D. M. and Liu, C. T., "SIF Distributions in Cracked Photoelastic Rocket Motor Studies; Preliminary Results," *Proceedings of the SEM Annual Conference on Experimental and Applied Mechanics,* pp. 105-108, June, 2001.

Smith, C. W., Constantinescu, D. M. and Liu, C. T., "Observations of Crack Turning by Optical Methods," *Advances in Computational Engineering and Sciences: Tech Science Press,* Chapter 9, Mechanics of Particulate Composites, 5 pages, August, 2001.

APPENDIX A- Frozen Stress Photoelasticity

When a transparent model is placed in a circularly polarized monochromatic light field and loaded, dark fringes will appear which are proportional to the applied load. These fringes are called stress fringes or isochromatics, and the magnitude of the maximum in-plane shear stress is a constant along a given fringe.

Some transparent materials exhibit mechanical diphase characteristics above a certain temperature, called the critical temperature (T_c). The material, while still perfectly elastic will exhibit a fringe sensitivity of about twenty times the value obtained at room temperature, and its modulus of elasticity will be reduced to about one six-hundredth of its room temperature value. By raising the model temperature above T_c, loading, and then cooling slowly to room temperature, the stress fringes associated with T_c will be retained when the material is returned to room temperature. Since the material is so much more sensitive to fringe generation above T_c than at room temperature, fringe recovery at room temperature upon unloading is negligible. The model may then be sliced without disturbing the "frozen in" fringe pattern and analyzed as a two-dimensional model but containing the three-dimensional effects. In the use of the method to make measurements near crack tips, due to the need to reduce loads above critical temperature to preclude large local deformations, and the use of thin slices, few stress fringes are available by standard procedures. To overcome this obstacle, a refined polariscope is employed to allow the tandem use of the Post and Tardy methods to increase the number of fringes available locally.

In fringe photographs, integral fringes are dark in a dark field and bright in a bright field.

Appendix B

Mode I Algorithm

Beginning with the Griffith-Irwin Equations, we may write, for Mode I, for the homogeneous case,

$$\sigma_{ij} = \frac{K_1}{(2\pi r)^{\frac{1}{2}}} f_{ij}(\theta) + \sigma^\circ_{ij} \qquad (i, j = n, z) \tag{1}$$

where:

σ_{ij} are components of stress
K_1 is SIF
r, θ are measured from crack tip (Fig. B-1)
σ°_{ij} are non-singular stress components

Then, along $\theta = \pi/2$, after truncating σ_{ij}

$$\tau^{max}_{nz} = \frac{K_1}{(8\pi r)^{\frac{1}{2}}} + \tau^\circ = \frac{K_{AP}}{(8\pi r)^{\frac{1}{2}}} \tag{2}$$

where:

$\tau^\circ = f(\sigma^\circ_{ij})$ and is constant over the data range
K_{AP} = apparent SIF
τ^{max}_{nz} = maximum shear stress in nz plane

Normalizing with respect to $\bar{\sigma}$,

$$\therefore \frac{K_{AP}}{\bar{\sigma}(\pi a)^{\frac{1}{2}}} = \frac{K_1}{\bar{\sigma}(\pi a)^{\frac{1}{2}}} + \frac{\sqrt{8}\tau^\circ}{\bar{\sigma}}\left(\frac{r}{a}\right)^{\frac{1}{2}} \tag{3}$$

where (Fig. B-1) a = crack length, and $\bar{\sigma}$ = remote normal stress

i.e $\frac{K_{AP}}{\bar{\sigma}(\pi a)^{\frac{1}{2}}}$ vs. $\sqrt{\frac{r}{a}}$ is linear.

From the Stress-Optic Law, $\tau_{nz}^{max} = nf/2t$ where,
n = stress fringe order,
f = material fringe value, and
t = specimen (or slice) thickness
then from Eq. 2

$$K_{AP} = \tau_{nz}^{max}(8\pi r)^{\frac{1}{2}} = \frac{nf}{2t}(8\pi r)^{\frac{1}{2}}$$

where K_{AP} (through a measure of n) and r become the measured quantities from the stress fringe pattern at different points in the pattern.

In the present study, instead of normalizing K with respect to $\bar{\sigma}(\pi a)^{1/2}$, we have selected $p_{sf}\sqrt{\pi a/Q}$ as the normalizing factor where $\sqrt{Q}$ is an elliptic integral of the second kind approximated here, as shown in Table I. An example of the determination of F_1 in Table I from test data is given in Fig. B-2.

Mixed Mode Algorithm

The mixed mode algorithm was developed (see Fig. B-3) by requiring that:

$$\lim_{\substack{r_m \to 0 \\ \theta_m \to \theta_m^\circ}} \left\{ (8\pi r_m)^{1/2} \frac{\delta(\tau)_{nz}^{max}}{\delta\theta} (K_1, K_2, r_m, \theta_m, \tau_{ij}) \right\} = 0 \qquad (4)$$

which leads to:

$$\left(\frac{K_2}{K_1}\right)^2 - \frac{4}{3}\left(\frac{K_2}{K_1}\right) cot\ 2\theta_m^\circ - \frac{1}{3} = 0 \qquad (5)$$

By measuring θ_m° which is approximately in the direction of the applied load, K_2/K_1 can be determined.

Then writing the stress optic law as:

$$\tau_{nz}^{max} = \frac{fn}{2t} = \frac{K_{AP}^*}{(8\pi r)^{\frac{1}{2}}}$$

where K_{ap}^* is the mixed mode SIF, one may plot $\frac{K_{AP}^*}{\bar{\sigma}(\pi a)^{\frac{1}{2}}}$ vs. $\sqrt{r/a}$ as before, locate a linear zone and extrapolate to $r = 0$ to obtain K^*. Knowing, K^*, K_2/K_1 and θ_m°, values of K_1 and K_2 may be determined since

$$K^* = [(K_1 sin\theta_m^\circ + 2K_2 cos\theta_m^0)^2 + (K_2 sin\theta_m^\circ)^2]^{\frac{1}{2}} \qquad (6)$$

Knowing K^* and θ_m°, K_1 & K_2 can be determined from Eqs. 5 and 6. Details are found in Smith and Kobayashi (1993).

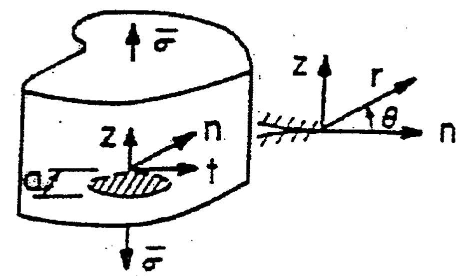

Fig. B-1 Near Tip Notation for Mode I.

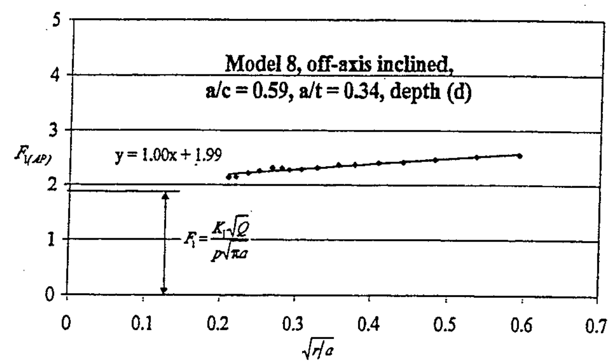

Fig. B-2: Determination of F_1 for Test Data.

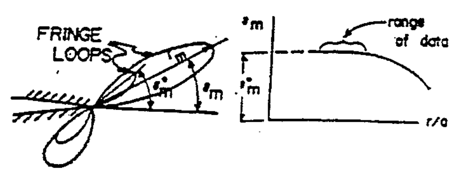

Fig. B-3: Determination of θ_m° for Mixed Mode

Table I DATA & RESULTS

Loads[1]	Crack Description[2] (dimensions in mm)	[3] F_i	
$P = 88.97$ N $p_{max} = 0.049$ MPa $p_{sf} = 0.035$ MPa	**Model 4** Off-axis inclined $a = 8.71$ $\Delta a = 2.18$ $c = 11.15$ $\Delta c = 3.02$ $a/c = 0.78$ $a/t = 0.23$	$F_1 = 1.90$ $F_2 = 0.48$	Notations: 1. P = axial compressive load p_{max} = internal pressure to grow crack p_{sf} = stress freezing pressure 2. a = crack depth; Δa = crack growth c = half length of crack in fin tip surface Δc = half crack growth in fin tip surface 3. $F_i = K_i\sqrt{Q}/p_{sf}\sqrt{\pi a}$ $i = 1,2$ at maximum depth $\sqrt{Q}$ = approximation of elliptic integral of second kind $Q = 1 + 1.464\left(\frac{a}{c}\right)^{1.65}$ $\quad \frac{a}{c} \leq 1$ All flaws were characterized as semi-elliptic flaws of depth a and length $2c$. However, off-axis cracks were neither perfectly semi-elliptic nor planar.
$P = 88.97$ N $p_{max} = 0.103$ MPa $p_{sf} = 0.049$ MPa	**Model 8-i** Off-axis inclined $a = 12.50$ $\Delta a = 3.4$ $c = 21.1$ $\Delta c = 10.4$ $a/c = 0.59$ $a/t = 0.34$	1.99	
$P = 88.97$ N $p_{max} = 0.049$ MPa $p_{sf} = 0.035$ MPa	**Model 6** Off-axis straight in $a = 11.60$ $\Delta a = 4.67$ $c = 17.00$ $\Delta c = 10.66$ $a/c = 0.68$ $a/t = 0.31$	1.72	
	Off-axis straight in $a = 11.23$ $\Delta a = 5.86$ $c = 13.00$ $\Delta c = 6.65$ $a/c = 0.86$ $a/t = 0.30$	1.86	
$P = 88.97$ N $p_{max} = 0.103$ MPa $p_{sf} = 0.049$ MPa	**Model 7** Off-axis straight in $a = 15.60$ $\Delta a = 10.0$ $c = 26.45$ $\Delta c = 17.57$ $a/c = 0.59$ $a/t = 0.42$	1.58	
	Off-axis straight in $a = 13.90$ $\Delta a = 4.05$ $c = 18.65$ $\Delta c = 10.17$ $a/c = 0.74$ $a/t = 0.37$	1.87	
$P = 88.97$ N $p_{max} = 0.103$ MPa $p_{sf} = 0.049$ MPa	**Model 8-s** Off-axis straight in $a = 7.90$ $\Delta a = 2.8$ $c = 13.35$ $\Delta c = 7.75$ $a/c = 0.59$ $a/t = 0.21$	1.93	
$P = 88.97$ N $p_{max} = 0.103$ MPa $p_{sf} = 0.049$ MPa	**Model 9** Off-axis straight in $a = 25.10$ $\Delta a = 18.7$ $c = 39.4$ $\Delta c = 33.8$ $a/c = 0.64$ $a/t = 0.68$	1.50	

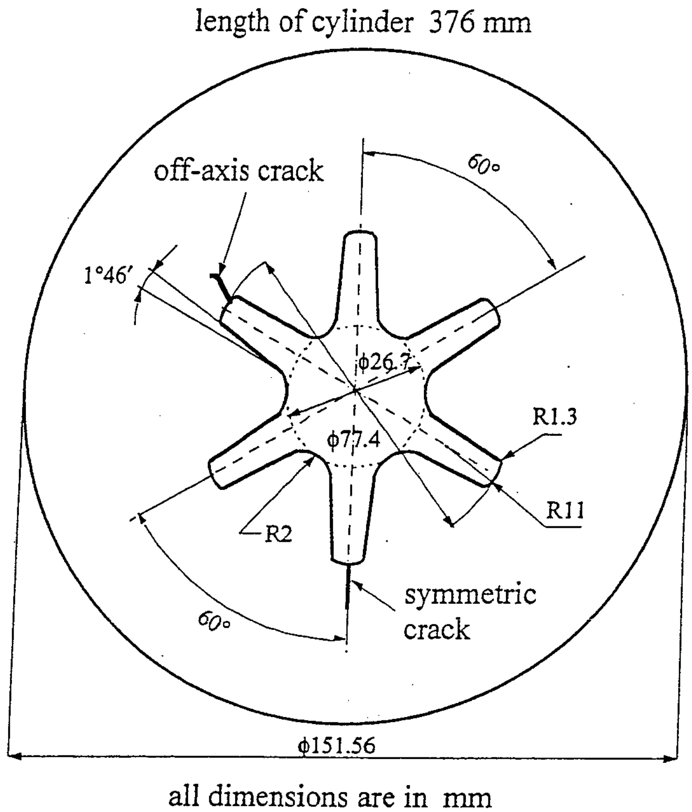

Fig. 1: Dimensions and Crack Locations in a Cross-Section of the Model

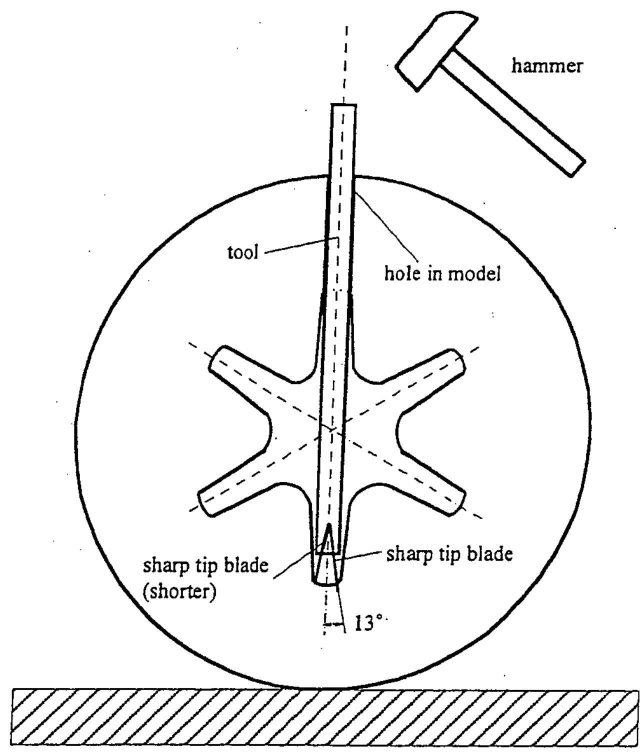

Fig. 2: Setup for Producing Off-Axis Starter Crack

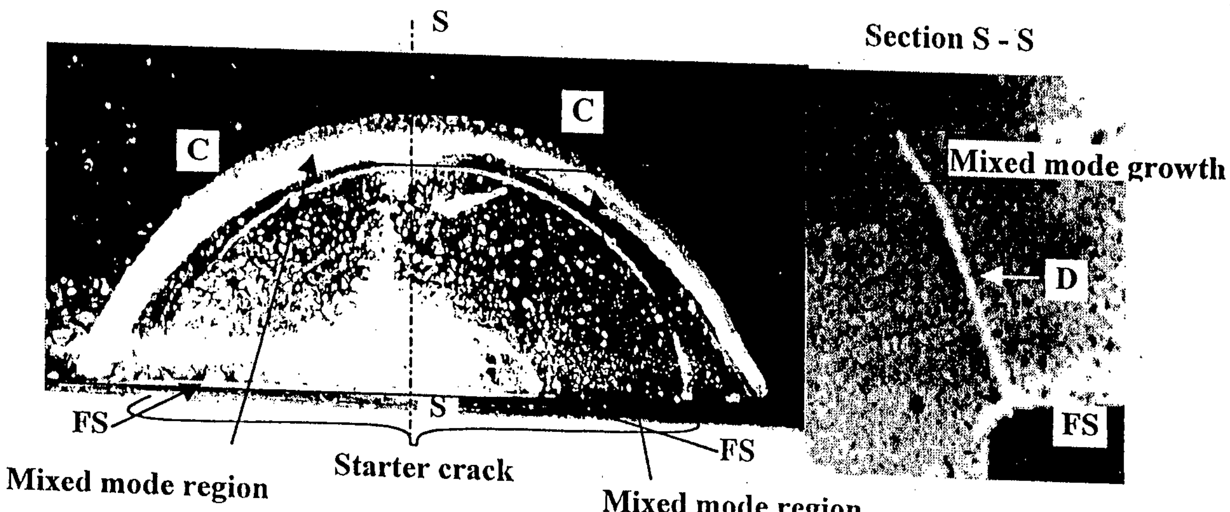

magnification factor: 4.22

Model 4 Off-Axis Inclined Crack Showing Starter Crack and Final Crack Front

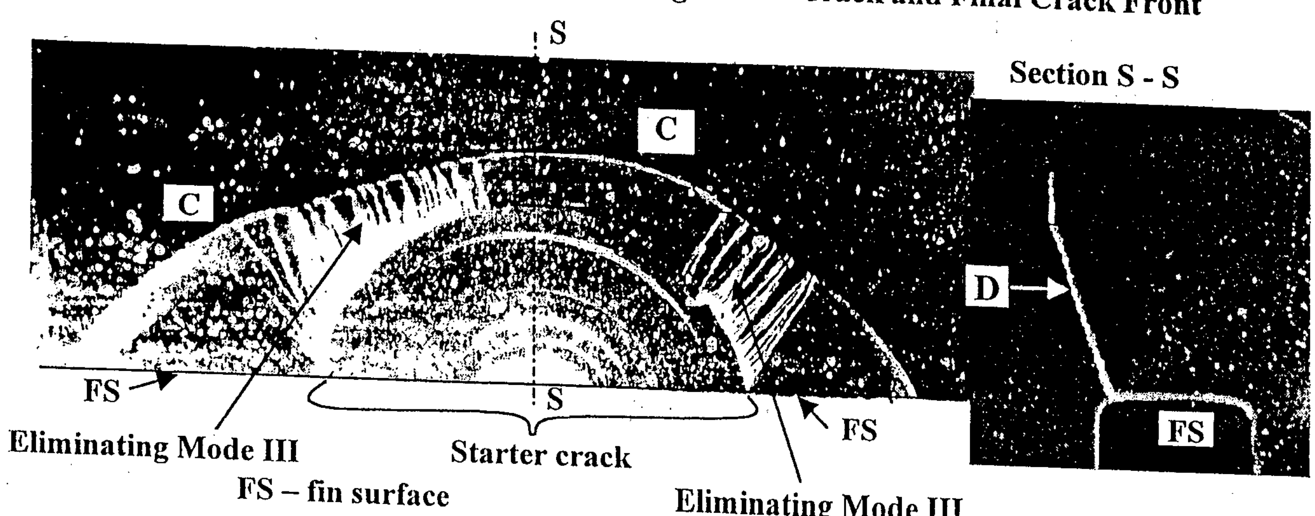

FS – fin surface
C – crack front
D – camera view of the photograph

magnification factor: 2.50

Model 8-i Off-Axis Inclined Crack Showing Starter Crack and Final Mode I Crack Front

Fig. 3: Typical Off-Axis Inclined Cracks (Blade Held Normal to Fin Surface)

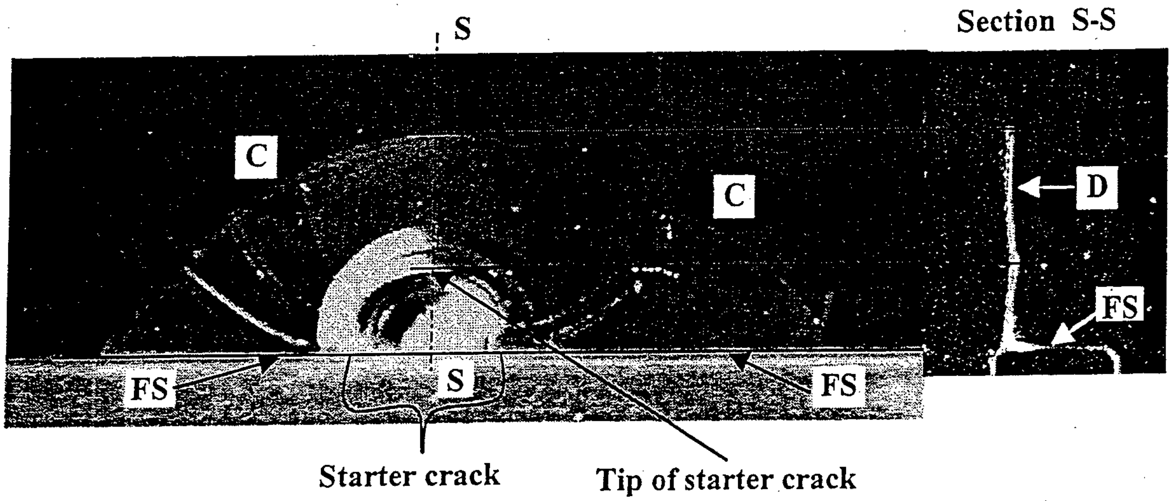

FS – fin surface
C – crack front
D – camera view of the photograph

magnification factor: 2.25

Model 7 Off-Axis Straight Crack Showing Starter Crack and Final Crack Front

Fig. 4: Typical Off-Axis Straight-in Crack (Blade Oriented Parallel to Fin Axis)

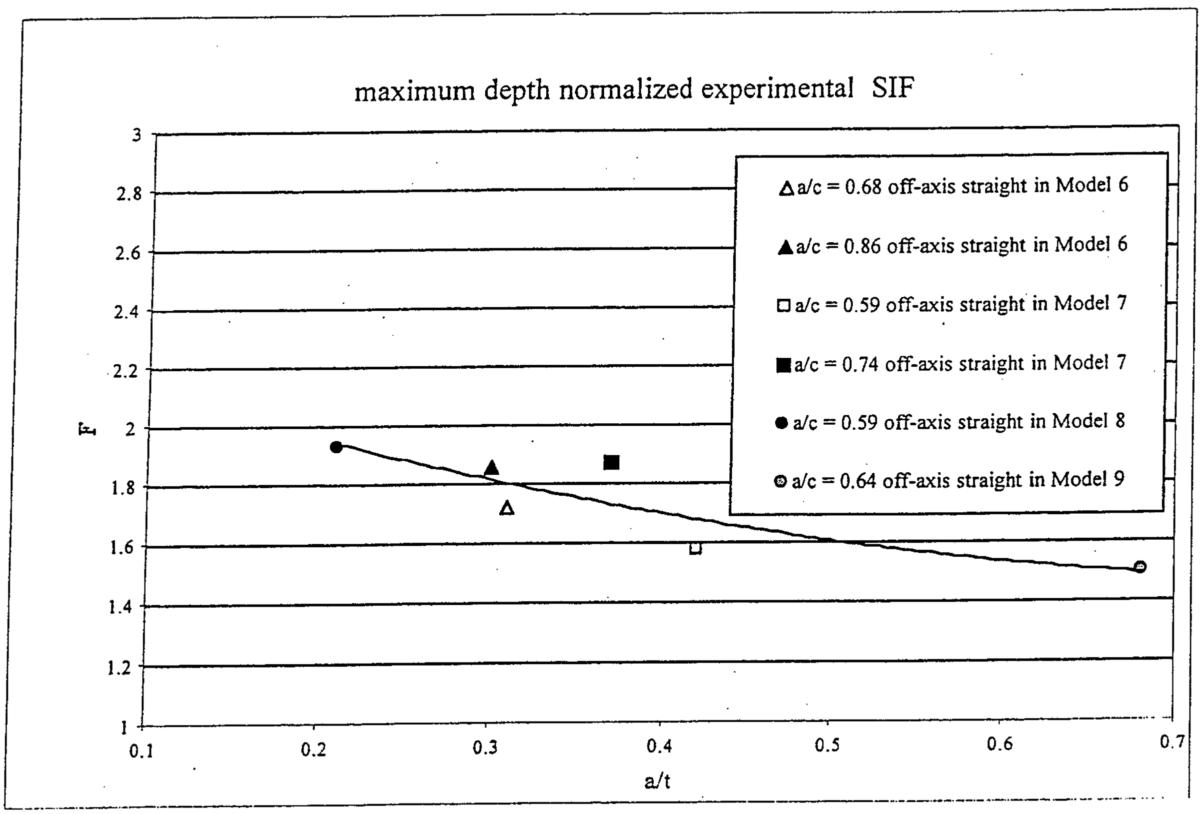

Fig. 5: Effect of Part-Through Crack Depth on Normalized SIF